Direct Characteristic-Function Tomography of Quantum States of the Trapped-Ion Motional Oscillator

C. Flühmann* and J. P. Home†
Institute for Quantum Electronics, ETH Zürich, Otto-Stern-Weg 1, 8093 Zürich, Switzerland

(Received 21 October 2019; accepted 26 June 2020; published 21 July 2020)

We implement direct readout of the symmetric characteristic function of quantum states of the motional oscillation of a trapped calcium ion. Suitably chosen internal state rotations combined with internal state-dependent displacements, based on bichromatic laser fields, map the expectation value of the real or imaginary part of the displacement operator to the internal states, which are subsequently read out. Combining these results provides full information about the symmetric characteristic function. We characterize the technique by applying it to a range of archetypal quantum oscillator states, including displaced and squeezed Gaussian states as well as two and three component superpositions of displaced squeezed states. For each, we discuss relevant features of the characteristic function and Wigner phase-space quasiprobability distribution. The direct reconstruction of these highly nonclassical oscillator states using a reduced number of measurements is an essential tool for understanding and optimizing the control of oscillator systems for quantum sensing and quantum information applications.

DOI: 10.1103/PhysRevLett.125.043602

Quantum state reconstruction is an important element enabling diagnosis and improvement of quantum control. As larger states come under experimental control the number of measurements required to perform state reconstruction becomes crucial [1]. Here, significant gains can be found by choosing the appropriate basis in which to make measurements [2]. Bosonic systems such as mechanical harmonic oscillators and electromagnetic field modes play a prominent role across quantum information [3,4], quantum sensing [5–8], and fundamental studies [9,10]. These have been prepared in a wide range of quantum states, including Fock, squeezed, and displaced states [11] and superpositions of these [12,13]. Particular focus has been placed on states involving superpositions of displaced states, for which the archetypal example is the "Schrödinger's cat" superposition of two displaced coherent states [14]. Studies include evolution under decoherence channels [15,16] as well as storage and manipulation of information in error-correction codes [4,17].

Prior works on oscillator state tomography include techniques based on homodyne measurements [18] and methods based on extraction of Fock state occupations, parity, and ground state occupation following displacements applied to the analyzed states [6,19–23]. These results are then processed to reconstruct states in the Fock state basis or to extract phase-space quasiprobability distributions, such as the Wigner and Husimi-$\mathcal{Q}$ function. When extracting quasiprobabilities, often a large amount of excess data is collected, such as extracting many Fock state occupations which are then reduced to a single parity value [2,19]. Direct parity measurements can be performed using strong dispersive Jaynes-Cummings interactions [21], but these require settings that are challenging on some platforms [24,25], and which often limit the quality and lifetime of larger field states [26–28]. Direct measurements of ground-state population allow the extraction of the $\mathcal{Q}$ function, but this is not well suited to analysis of catlike states since quantum interference effects are exponentially suppressed with the separation of the displaced wave packets [29].

A complete description of the quantum state is also given by the characteristic function of the quasiprobability distributions [36]. The symmetric characteristic function is defined as:

$$\chi(\beta) = \langle \hat{\mathcal{D}}(\beta) \rangle, \tag{1}$$

with $\hat{\mathcal{D}}(\beta) = e^{\beta \hat{a}^\dagger - \beta^* \hat{a}}$ being a shift operator by the complex amount β [37]. Here $\hat{a}$ is the usual harmonic oscillator destruction operator and $\langle \cdot \rangle = \langle \psi_{\mathrm{os}} | \cdot | \psi_{\mathrm{os}} \rangle$ denotes the expectation value evaluated on the analyzed state $|\psi_{\mathrm{os}}\rangle$. The quasiprobability distributions can be obtained from the characteristic function $\chi(\beta)$ using a two-dimensional Fourier transform of $\chi(\beta)$ [36]:

$$\mathcal{W}_l(\gamma) = \frac{1}{\pi^2} \int \chi(\beta) e^{l|\beta|^2/2} e^{\gamma \beta^* - \gamma^* \beta} d^2\beta. \tag{2}$$

For $l = 0$ this gives the Wigner function, for $l = -1$ the Husimi-$\mathcal{Q}$ function, and for $l = 1$ the Glauber-Sudarshan P representation. The P representation can become singular, while the Wigner and $\mathcal{Q}$ function are both bounded. Thus only the latter two are commonly used in experiments [2,4,16,18–20,22–25,38]. Methods to directly reconstruct $\chi(\beta)$ have been proposed as early as 1995 [39,40] and have

been used for 1D reconstruction of wave functions [41–44] as well as 2D reconstruction of Fock and thermal states [45]. It is important to note that single or few point measurements of the characteristic and Wigner functions provide different information. They correspond for example to stabilizer readouts of different bosonic encodings [3,4]. Furthermore, expectation values of powers of creation and destruction operators [36] are given by derivatives of the characteristic function around the origin

$$\langle \hat{a}^{\dagger m} \hat{a}^n \rangle_S = \left(\frac{\partial}{\partial \beta}\right)^m \left(-\frac{\partial}{\partial \beta^*}\right)^n \chi(\beta)|_{\beta=0}.$$

Here the subscript S denotes symmetric operator ordering [29]. Obtaining the same information requires integration of the Wigner function over the complete phase space.

In this Letter we perform direct reconstruction of the characteristic function of a trapped-ion motional oscillator state, and illustrate its use by applying it to a squeezed state, a displaced-squeezed state, a squeezed Schödinger's cat state [2,46], and a GKP codeword consisting of three superposed displaced-squeezed states [3,17]. All reconstructions are in close agreement with the independent calibrations of the measured states, but reveal small significant discrepancies in the experimentally set parameters, which could be used for future improvements in state control. Due to the direct nature of the reconstruction method, we find a reduction in data taking time of more than a factor of 20 relative to methods we used previously [29].

The oscillator used in the experiments is the axial motional mode of a single trapped $^{40}Ca^+$ ion with a frequency of around $\omega_m \approx 2\pi \times 1.9$ MHz. All experiments were performed at room temperature in a segmented linear Paul trap consisting out of a stack of gold-coated wavers [47]. The motional mode is controlled and read out via the internal electronic levels $|\downarrow\rangle \equiv |^2S_{1/2}, m_j = 1/2\rangle$, and $|\uparrow\rangle \equiv |^2D_{5/2}, m_j = 3/2\rangle$. The quantum circuit used for reconstruction is given in Fig. 1. At the beginning of each experiment the axial motional mode is initialized to a given oscillator state $|\psi_{\rm os}\rangle$, which we aim to reconstruct. The initial electronic state is prepared to $|\uparrow\rangle$. Then a resonant carrier rotation $\hat{R}(\theta, \phi) = \cos(\theta/2)\mathbb{1} - i\sin(\theta/2)[\cos(\phi)\hat{X} + \sin(\phi)\hat{Y}]$ is applied to the internal states. Here θ is proportional to the laser pulse duration and amplitude, while ϕ is given by the laser phase, $\mathbb{1}$ is the identity, while $\hat{X} \equiv |\uparrow\rangle\langle\downarrow| + |\downarrow\rangle\langle\uparrow|$, $\hat{Y} \equiv -i|\uparrow\rangle\langle\downarrow| + i|\downarrow\rangle\langle\uparrow|$, and $\hat{Z} = |\uparrow\rangle\langle\uparrow| - |\downarrow\rangle\langle\downarrow|$ are the Pauli matrices acting on the internal states. The rotation is followed by application of an internal state-dependent force (SDF) based on a bichromatic laser pulse realizing the operation $\hat{\mathcal{D}}[\beta(t)\hat{X}/2]$, where $\beta(t)/2 = \eta\Omega t e^{-i\Delta\varphi/2}$ [48]. Here $\eta \simeq 0.05$ denotes the Lamb-Dicke parameter [49], while the Rabi frequency Ω and $\Delta\varphi$ are controlled via the amplitude and relative phases of the bichromatic laser fields. The SDF shifts the oscillator state with a direction dependent on the $\hat{X}$ eigenvalue of the internal states. Finally the internal state is read out using resonant fluorescence [49]. This circuit can be viewed as performing an indirect measurement of the oscillator via the internal states. The Pauli $\hat{Z}$ expectation value follows [50–52]:

$$\begin{aligned}\langle \hat{Z} \rangle &= \langle e^{i\theta}\hat{\mathcal{D}}(-\beta) + e^{-i\theta}\hat{\mathcal{D}}(\beta)\rangle/2 \\ &= \cos(\theta)\mathrm{Re}[\chi(\beta)] + \sin(\theta)\mathrm{Im}[\chi(\beta)]. \end{aligned} \quad (3)$$

The imaginary part of the characteristic function is measured with a carrier rotation $\theta = \pi/2$, while the real part is obtained by switching off the rotation ($\theta = 0$). In the following we will use the short notation $\chi(\beta)$ if the analyzed state $|\psi_{\rm os}\rangle$ is unambiguous and $\chi(\beta, |\psi_{\rm os}\rangle)$ where the specific state is important.

The characteristic function is complex valued and Hermitian $\chi(\beta)^* = \chi(-\beta)$ and thus any half of the complex space covered by β is sufficient for a complete measurement. Therefore only a single measurement setting (repeated to average quantum projection noise) is required to obtain one characteristic function point. In our experiment this represents a reduction of two orders of magnitude of required readouts over previous work on Wigner function reconstruction [2]. In the following experiments, we sample the states on an uniformly spaced square grid in order to learn more about the method and obtain pictures of the quantum mechanical oscillator states.

We start our study by analyzing displaced and squeezed vacuum states $|\psi_{\rm os}\rangle = |\delta, re^{i\vartheta}\rangle = \hat{\mathcal{D}}(\delta)\hat{\mathcal{S}}(re^{i\vartheta})|0\rangle$. Here the phase-space squeezing operator is defined as $\hat{\mathcal{S}}(\xi = re^{i\vartheta}) = \exp[(-\xi\hat{a}^{\dagger 2} + \xi^*\hat{a}^2)/2]$ and $|0\rangle$ denotes the oscillator ground state. Displaced squeezed states are prepared experimentally by first cooling the motion of the ion into a squeezed state $|re^{i\vartheta}\rangle = \hat{\mathcal{S}}(re^{i\vartheta})|0\rangle$ using reservoir engineering [53] and subsequently applying an oscillating voltage to one of our trap electrodes resonant with the ion's motional frequency implementing the shift $\hat{\mathcal{D}}(\delta)$. Figure 2 shows the extracted characteristic function obtained from two states with squeezing parameters $r_c = 0.93 \pm 0.02$ and $\vartheta_c = 0$ and displacements $\delta_c = 0$ [Figs. 2(a) and 2(b)] and $\delta_c = 0.78 \pm 0.05$ [Figs. 2(d) and 2(e)]. Here and elsewhere in this manuscript quoted values with subscript c were either set to this value (no error bar) or

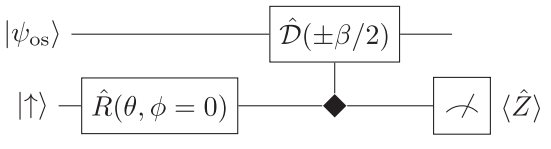

FIG. 1. Characteristic function readout of the oscillator state $|\psi_{\rm os}\rangle$. A carrier rotation $\hat{R}(\theta, \phi = 0)$ is applied to the internal states initialized to $|\uparrow\rangle$, subsequently the oscillator is displaced by $\hat{\mathcal{D}}(\pm\beta/2)$, where the sign depends on the internal states in the $\hat{X}$ basis (diamond symbol); finally, the internal states are readout.

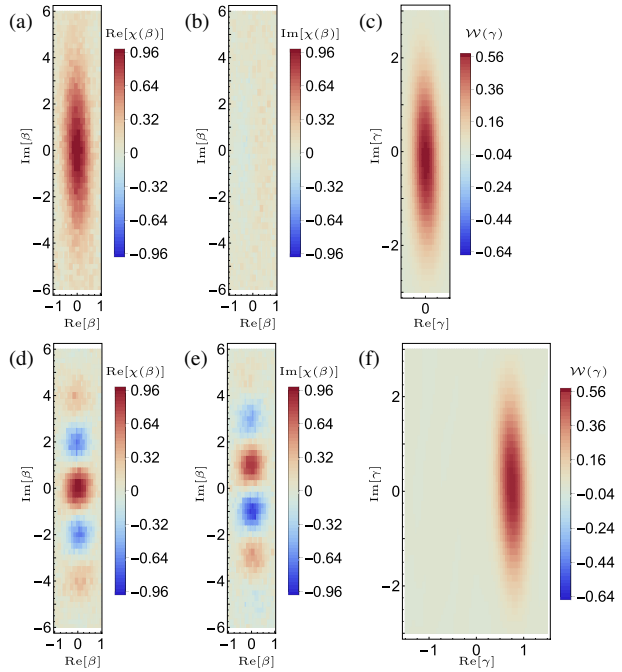

FIG. 2. Reconstruction of displaced squeezed oscillator states $|\delta, re^{i\vartheta}\rangle = \hat{\mathcal{D}}(\delta)\hat{\mathcal{S}}(re^{i\vartheta})|0\rangle$ with $r_c = 0.93 \pm 0.02$ and orientations chosen to be $\vartheta_c = 0$. (a)–(c) shows the squeezed vacuum state with $\delta_c = 0$, while (d)–(f) reconstruct the displaced squeezed state with $\delta_c = 0.78 \pm 0.05$. The real and imaginary readouts of the characteristic function (a) and (b), (d) and (e) show measurement data, while the Wigner function (c) and (f) was obtained performing the two-dimensional Fourier transform given in Eq. (2).

are values obtained from independent calibration measurements [29].

The form of the measured results qualitatively follows the expectation from theory [29]. For tomography in general, a common approach would be to find the physically constrained characteristic function that is closest to the measurement [54,55]. However identifying a suitable basis set is nontrivial and appears rather indirect. As an alternative, we instead look for the closest pure state which might reproduce the data, using a model which takes account of known sources of imperfection. We fit the measurement data to the functional form

$$E(\beta) = \chi(\beta)(1 - |b|) + b, \tag{4}$$

with $\chi(\beta)$ as the expected characteristic function based on a small set of parameters $\{\zeta\}$, and b a bias parameter that accounts for state-preparation and measurement errors of the internal state (SPAM) [29]. In each case b and $\{\zeta\}$ are floated. For pure displaced-squeezed states the characteristic function is

$$\chi(\beta, |\delta, re^{i\vartheta}\rangle) = e^{-|\beta\cosh(r)+\beta^* e^{i\vartheta}\sinh(r)|^2/2} e^{\beta\delta^* - \beta^*\delta} \tag{5}$$

and $\{\zeta\} = \{\delta, r, \vartheta\}$.

We rate the quality of the fit based on a standard reduced chi-squared function $c_r = 1/(N-\nu)\sum_{i=1}^{N}[\chi(\beta_i) - E(\beta_i)]^2/\sigma_i^2$ where ν denotes the number of fitting parameters, N the total number of measurements, $\chi(\beta_i)$ the measurement result at the phase-space point β_i, and σ_i the standard error on the mean (s.e.m.) of each point. For the (displaced) squeezed vacuum states the fitted parameters yield ($c_r = 1.07$) $c_r = 1.09$, which is a significant improvement over the values ($c_r = 1.78$), $c_r = 1.82$ obtained using the independently calibrated values. For both states the fit revealed a small tilt $\vartheta = 0.044 \pm 0.002$ together with a discrepancy in the shift $|\mathrm{Im}[\delta]| = 0.149 \pm 0.006$. In addition a bias $b = 3.05 \pm 0.07\%$ was found, which was explained due to poorly calibrated internal-state preparation for this data set. Quoted values above denote the average of the fitted parameters for the two states. A complete list of all parameters can be found in Table I of the Supplemental Material [29]. The tilt ϑ is only visible in the large data set and indicates the potential for improving the SDF and squeezed state phase calibration in the future. The cause of the small shift along the imaginary axis is currently unclear.

To obtain a Wigner function for our states, we perform the discrete version of the Fourier transform (DFT) given in Eq. (2) with $l = 0$. Prior to the DFT, we remove the bias b and zero pad the data outside the measurement range, and additionally resample the data on an equidistant grid. Results are shown in Figs. 2(c) and 2(f), respectively. The numerical errors occurring due to the additional data processing can be estimated using sampling of ideal states [29]. The average magnitude of the discrepancy over all sampled points of the Wigner function is found for the states above to be 0.29%. Comparison of the Wigner and characteristic functions show for both states that these quantities exhibit a smaller extent and hence a reduced uncertainty along $\mathrm{Re}(\gamma)$ versus $\mathrm{Im}(\gamma)$. However the displacement $\hat{\mathcal{D}}(\delta)$ has different effects, shifting the Wigner function while appearing in the characteristic function as an oscillation of the function in the direction perpendicular to the shift. The latter is due to geometric phases $\hat{\mathcal{D}}(\beta)\hat{\mathcal{D}}(\delta) = \exp[(\beta\delta^* - \beta^*\delta)/2]\hat{\mathcal{D}}(\delta + \beta)$ which occur when displacement operators are combined.

Displaced and squeezed states belong to the category of Gaussian oscillator states [56,57]. Non-Gaussian states, for example "Schrödinger's cat states" [14], can produce negative values for the Wigner function, which makes its interpretation as a probability density in phase-space impossible. A cat state can be realized as a superposition of two displaced squeezed states

$$|\psi_{\mathrm{os}}\rangle \propto \hat{\mathcal{D}}(\delta)[\hat{\mathcal{D}}(-\alpha/2) + \hat{\mathcal{D}}(\alpha/2)]|re^{i\vartheta}\rangle, \tag{6}$$

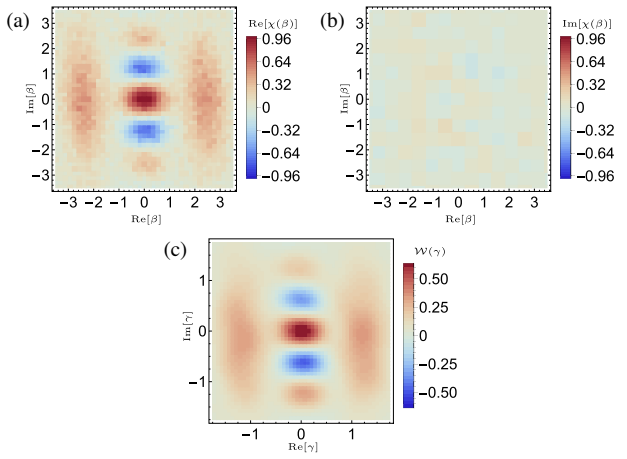

FIG. 3. Squeezed cat state reconstruction $[\hat{\mathcal{D}}(-\alpha/2) + \hat{\mathcal{D}}(\alpha/2)]|re^{i\vartheta}\rangle$ with $\alpha_c = 2.42 \pm 0.01$, $r_c = 0.58 \pm 0.02$. The real and imaginary part of the characteristic function measurement are given in parts (a) and (b) while part (c) shows the Wigner function found via DFT.

which we create using the circuit given in Fig. 1 with a squeezed oscillator state as input and postselecting on the measurement result [2,46]. Experimental reconstruction of the characteristic function of such a superposition state with $\alpha_c = 2.42 \pm 0.01$, $r_c = 0.58 \pm 0.02$, $\vartheta_c = \delta_c = 0$ is shown in Fig. 3. The acquisition time for this measurement was ≈ 6 h, which includes repeated recalibration of the SDF Rabi frequency Ω. Both the duration of the SDF used for the preparation of the cat state as well as during the analysis were updated accordingly. This leads to additional fluctuations on the input state preparation due to the calibration accuracy, when compared to shorter experiments. We again fit the measurement data to the expected analytic functional form [29], including the bias b, and obtain a reduced chi squared of $c_r = 1.40$, which is a reduction relative to that of the calibrated values $c_r = 1.71$. The fit parameters $\mathrm{Re}[\alpha] = 2.396 \pm 0.004$, $r = 0.543 \pm 0.005$ are close to the calibrated values. A substantially smaller shift $|\delta| = 0.04 \pm 0.01$ and bias $b = 0.9 \pm 0.1\%$ was obtained in this case compared to the displaced-squeezed states. However the tilt $\vartheta = 0.110 \pm 0.007$ increased.

The intrinsic quantum mechanical feature of the cat state is given by the stable phase relation between the differently displaced parts. For the ideal calibrated state with $\delta_c = 0$ this is often confirmed by measuring the value of the parity ideally given by $\langle\hat{\mathcal{P}}\rangle = 1$ where $\hat{\mathcal{P}} \equiv (-1)^{\hat{a}^\dagger \hat{a}}$ [36]. This is closely related to the value of the Wigner function at the origin and thus to the integral of the characteristic function over the full space

$$\langle\hat{\mathcal{P}}\rangle = \frac{\pi}{2}\mathcal{W}(0) = \frac{1}{2\pi}\int \mathrm{Re}[\chi(\beta)]d^2\beta. \tag{7}$$

Performing the Fourier transform of the characteristic function measurements as above gives a parity of $\langle\hat{\mathcal{P}}\rangle = 0.98$ (we find the numerical-analysis DFT error in this case to be 0.70%, see [29]). In this estimation the bias due to SPAM plays an important role. Without removing the fitted value of $b = 0.9 \pm 0.1\%$ from all data we find a value of $\langle\hat{\mathcal{P}}\rangle = 0.90$. This example shows that any constant offset in the data leads to large error in a measurement of the parity. It is worth noting that the close similarity between the characteristic function and the Wigner function for the squeezed-cat state superposition is misleading. The oscillation in the Wigner function along the imaginary axis indicate the presence of a stable phase relation between the two displaced components. In contrast the oscillations along the imaginary axis in the characteristic function would be identical for the mixture $\rho_{\mathrm{mix}} \propto |\alpha/2, \xi\rangle\langle\alpha/2, \xi| + |-\alpha/2, \xi\rangle\langle-\alpha/2, \xi|$. In case of the characteristic function the phase relation is confirmed by the peaks at $\mathrm{Re}[\beta] = \pm\alpha$, which in contrast to the parity measurement only requires a single readout.

After testing the characteristic function method we tackle partial reconstruction of a three-component superposition $|\psi_{\mathrm{os}}\rangle \propto \hat{\mathcal{D}}(\delta)[\hat{\mathcal{D}}(-l) + 2 \cdot \mathbb{1} + \hat{\mathcal{D}}(l)]|re^{i\vartheta}\rangle$ with $l_c = 2.50 \pm 0.05$ and $r_c = 0.93 \pm 0.03$, $\delta_c = \vartheta_c = 0$, which is an approximate GKP code state [17,58]. Figure 4 shows the characteristic function measurement results. In this case only the positive quadrant of the real part was measured, which is indicated by the dashed box in Fig. 4(a). From these measurements the parity is estimated to be $\langle\hat{\mathcal{P}}\rangle \approx 0.95 \pm 0.02$ with the error bar denoting the error due

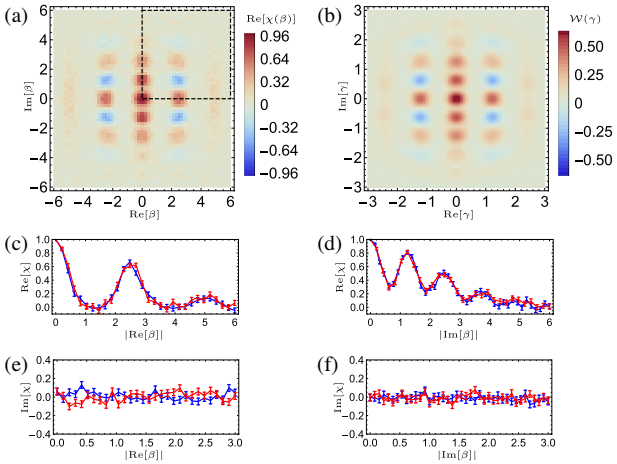

FIG. 4. Reconstruction of a three component superposition state $\hat{\mathcal{D}}(\delta)[\hat{\mathcal{D}}(-l) + 2 \cdot \mathbb{1} + \hat{\mathcal{D}}(l)]|re^{i\vartheta}\rangle$. The state was calibrated to $l_c = 2.50 \pm 0.05$, $r_c = 0.93 \pm 0.03$ and $\delta_c = \vartheta_c = 0$. In order to reduce experimental run time only the positive quadrant of $\mathrm{Re}[\chi(\beta)]$ was measured, indicated by the dashed box in (a). This was combined with three mirrored versions of itself to visualize the full state. (b) Shows the Wigner function obtained via DFT. In (c)–(f) we confirm the symmetries of the state with scans along the complete axes $\mathrm{Re}[\beta]$ and $\mathrm{Im}[\beta]$. Errors are given as s.e.m. We overlay results of the negative axis (blue) with results of the positive axis (red) by plotting measurements as a function of $|\beta|$.

to the uncertainty in b. This is close to 1 and thus constrains the value of the imaginary part to be close to zero throughout. The expected symmetries of the state are additionally confirmed by measuring the full imaginary and real phase-space axes, results are shown in Figs. 4(c)–4(f), respectively. The measurements confirm that the essential information about the reconstructed state is captured by the positive quadrant. Figure 4(e) however shows a small systematic close to zero, which only partially follows the expected odd symmetry of $\mathrm{Im}[\chi]$. This might be due to small uncontrolled and partially fluctuating displacements of the state from the origin δ. Figure 4(b) shows the Wigner function obtained using a DFT. In this case we obtain an average expected error from the numerical analysis of 0.45%. For the GKP state a fit using Eq. (4) obtains a reduction of the reduced chi square to $c_r = 1.58$ compared to $c_r = 2.05$ for the calibrated values. The primary discrepancy between calibration and fit is again a tilt of the squeezing direction $\vartheta = 0.103 \pm 0.008$. All other parameters are within the calibration error bars [29].

We have implemented direct, simple, and versatile reconstruction of the symmetric characteristic function and demonstrated its capabilities by analyzing displaced squeezed states and superpositions of these states. We focused our discussion on potential improvements of experimental control based on the large reconstruction data set revealing discrepancies between calibrations and fits. However it is also worth pointing out that these discrepancies are small: the square fidelities between calibrated and fitted pure states are above 0.98 for all four analyzed states including the GKP code word [29]. Possible extensions of this work include extracting the values of $\langle n \rangle$, $g^2(0)$, $\langle \hat{a}^{\dagger m} \hat{a}^n \rangle_S$ from a few measurement settings made close to the origin. This requires numerical techniques optimized for estimating derivatives from a sparsely sampled noisy signal [59–61]. Other extensions include the use of optimized sampling patterns [1,62] and the use of feedback to improve the quality of state preparation. The basic idea of utilizing qubit state-dependent shifts for reconstruction of a bosonic degree of freedom is applicable to a wide variety of spin-boson systems. For example, in parallel work on GKP states [58] characteristic function reconstructions were used for a microwave cavity with a weak dispersive interaction.

We thank M. Marinelli, V. Negnevitsky, and T. Behrle for contributions to the apparatus, and T.-L. Nguyen for useful discussions. We acknowledge support from the Swiss National Science Foundation through the National Center of Competence in Research for Quantum Science and Technology (QSIT) Grant No. 51NF40–160591.

*christa.fluhmann@yale.edu
†jhome@phys.ethz.ch

[1] C. Shen, R. W. Heeres, P. Reinhold, L. Jiang, Y.-K. Liu, R. J. Schoelkopf, and L. Jiang, Phys. Rev. A **94**, 052327 (2016).
[2] D. Kienzler, C. Flühmann, V. Negnevitsky, H.-Y. Lo, M. Marinelli, D. Nadlinger, and J. P. Home, Phys. Rev. Lett. **116**, 140402 (2016).
[3] D. Gottesman, A. Kitaev, and J. Preskill, Phys. Rev. A **64**, 012310 (2001).
[4] N. Ofek, A. Petrenko, R. Heeres, P. Reinhold, Z. Leghtas, B. Vlastakis, Y. Liu, L. Frunzio, S. M. Girvin, L. Jiang, M. Mirrahimi, M. H. Devoret, and R. J. Schoelkopf, Nature (London) **536**, 441 (2016).
[5] J. Aasi, J. Abadie, B. P. Abbott, R. Abbott, T. D. Abbott, M. R. Abernathy, C. Adams, T. Adams, P. Addesso, R. X. Adhikari *et al.*, Nat. Photonics **7**, 613 (2013).
[6] J. Zhang, M. Um, D. Lv, J.-N. Zhang, L.-M. Duan, and K. Kim, Phys. Rev. Lett. **121**, 160502 (2018).
[7] V. Meyer, M. A. Rowe, D. Kielpinski, C. A. Sackett, W. M. Itano, C. Monroe, and D. J. Wineland, Phys. Rev. Lett. **86**, 5870 (2001).
[8] K. C. McCormick, J. Keller, S. C. Burd, D. J. Wineland, A. C. Wilson, and D. Leibfried, Nature (London) **572**, 86 (2019).
[9] A. S. Arora and A. Asadian, Phys. Rev. A **92**, 062107 (2015).
[10] A. Asadian, C. Budroni, F. E. S. Steinhoff, P. Rabl, and O. Gühne, Phys. Rev. Lett. **114**, 250403 (2015).
[11] D. M. Meekhof, C. Monroe, B. E. King, W. M. Itano, and D. J. Wineland, Phys. Rev. Lett. **76**, 1796 (1996).
[12] C. Monroe, D. M. Meekhof, B. E. King, and D. J. Wineland, Science **272**, 1131 (1996).
[13] M. Hofheinz, H. Wang, M. Ansmann, R. C. Bialczak, E. Lucero, M. Neeley, A. D. O'Connell, D. Sank, J. Wenner, J. M. Martinis, and A. N. Cleland, Nature (London) **459**, 546 (2009).
[14] E. Schrödinger, Naturwissenschaften **23**, 807 (1935).
[15] Q. A. Turchette, C. J. Myatt, B. E. King, C. A. Sackett, D. Kielpinski, W. M. Itano, C. Monroe, and D. J. Wineland, Phys. Rev. A **62**, 053807 (2000).
[16] H. Wang, M. Hofheinz, M. Ansmann, R. C. Bialczak, E. Lucero, M. Neeley, A. D. O'Connell, D. Sank, M. Weides, J. Wenner, A. N. Cleland, and J. M. Martinis, Phys. Rev. Lett. **103**, 200404 (2009).
[17] C. Flühmann, T. L. Nguyen, M. Marinelli, V. Negnevitsky, K. Mehta, and J. P. Home, Nature (London) **566**, 513 (2019).
[18] A. I. Lvovsky and M. G. Raymer, Rev. Mod. Phys. **81**, 299 (2009).
[19] D. Leibfried, D. M. Meekhof, B. E. King, C. Monroe, W. M. Itano, and D. J. Wineland, Phys. Rev. Lett. **77**, 4281 (1996).
[20] P. Bertet, A. Auffeves, P. Maioli, S. Osnaghi, T. Meunier, M. Brune, J. M. Raimond, and S. Haroche, Phys. Rev. Lett. **89**, 200402 (2002).
[21] L. G. Lutterbach and L. Davidovich, Phys. Rev. Lett. **78**, 2547 (1997).
[22] B. Vlastakis, G. Kirchmair, Z. Leghtas, S. E. Nigg, L. Frunzio, S. M. Girvin, M. Mirrahimi, M. H. Devoret, and R. J. Schoelkopf, Science **342**, 607 (2013).
[23] C. Guerlin, J. Bernu, S. Deléglise, C. Sayrin, S. Gleyzes, S. Kuhr, M. Brune, J.-M. Raimond, and S. Haroche, Nature (London) **448**, 889 (2007).
[24] S. Ding, G. Maslennikov, R. Hablützel, H. Loh, and D. Matsukevich, Phys. Rev. Lett. **119**, 150404 (2017).

[25] D. Lv, S. An, M. Um, J. Zhang, J.-N. Zhang, M. S. Kim, and K. Kim, Phys. Rev. A **95**, 043813 (2017).
[26] D. I. Schuster, A. A. Houck, J. A. Schreier, A. Wallraff, J. M. Gambetta, A. Blais, L. Frunzio, J. Majer, B. Johnson, M. H. Devoret, S. M. Girvin, and R. J. Schoelkopf, Nature (London) **445**, 515 (2007).
[27] S. E. Nigg, H. Paik, B. Vlastakis, G. Kirchmair, S. Shankar, L. Frunzio, M. H. Devoret, R. J. Schoelkopf, and S. M. Girvin, Phys. Rev. Lett. **108**, 240502 (2012).
[28] S. Rosenblum, P. Reinhold, M. Mirrahimi, L. Jiang, L. Frunzio, and R. J. Schoelkopf, Science **361**, 266 (2018).
[29] See the Supplemental Material at http://link.aps.org/supplemental/10.1103/PhysRevLett.125.043602 for further information, which includes Refs. [30–35].
[30] Z. Leghtas, G. Kirchmair, B. Vlastakis, R. J. Schoelkopf, M. H. Devoret, and M. Mirrahimi, Phys. Rev. Lett. **111**, 120501 (2013).
[31] M. H. Michael, M. Silveri, R. T. Brierley, V. V. Albert, J. Salmilehto, L. Jiang, and S. M. Girvin, Phys. Rev. X **6**, 031006 (2016).
[32] S. Ryl, J. Sperling, and W. Vogel, Phys. Rev. A **95**, 053825 (2017).
[33] C. Langer, R. Ozeri, J. D. Jost, J. Chiaverini, B. DeMarco, A. Ben-Kish, R. B. Blakestad, J. Britton, D. B. Hume, W. M. Itano, D. Leibfried, R. Reichle, T. Rosenband, T. Schaetz, P. O. Schmidt, and D. J. Wineland, Phys. Rev. Lett. **95**, 060502 (2005).
[34] G. S. Agarwal, *Quantum Optics* (Cambridge University Press, Cambridge, England, 2012).
[35] P. Král, J. Mod. Opt. **37**, 889 (1990).
[36] S. M. Barnett and P. M. Radmore, *Methods in Theoretical Quantum Optics* (Oxford University Press, Oxford, 2002).
[37] W. P. Schleich, in *Quantum Optics in Phase Space* (Wiley-VCH Verlag GmbH & Co. KGaA, New York, 2005), pp. 171–188.
[38] C. Wang, Y. Y. Gao, P. Reinhold, R. W. Heeres, N. Ofek, K. Chou, C. Axline, M. Reagor, J. Blumoff, K. M. Sliwa, L. Frunzio, S. M. Girvin, L. Jiang, M. Mirrahimi, M. H. Devoret, and R. J. Schoelkopf, Science **352**, 1087 (2016).
[39] S. Wallentowitz and W. Vogel, Phys. Rev. Lett. **75**, 2932 (1995).
[40] S.-B. Zheng, X.-W. Zhu, M. Feng, and L. Shi, Phys. Rev. A **62**, 035801 (2000).
[41] J. Casanova, C. E. López, J. J. García-Ripoll, C. F. Roos, and E. Solano, Eur. Phys. J. D **66**, 222 (2012).
[42] R. Gerritsma, B. P. Lanyon, G. Kirchmair, F. Zähringer, C. Hempel, J. Casanova, J. J. García-Ripoll, E. Solano, R. Blatt, and C. F. Roos, Phys. Rev. Lett. **106**, 060503 (2011).
[43] R. Gerritsma, G. Kirchmair, F. Zähringer, E. Solano, R. Blatt, and C. F. Roos, Nature (London) **463**, 68 (2010).
[44] F. Zähringer, G. Kirchmair, R. Gerritsma, E. Solano, R. Blatt, and C. F. Roos, Phys. Rev. Lett. **104**, 100503 (2010).
[45] K. G. Johnson, B. Neyenhuis, J. Mizrahi, J. D. Wong-Campos, and C. Monroe, Phys. Rev. Lett. **115**, 213001 (2015).
[46] H.-Y. Lo, D. Kienzler, L. de Clercq, M. Marinelli, V. Negnevitsky, B. Keitch, and J. Home, Nature (London) **521**, 336 (2015).
[47] D. Kienzler, Ph.d. thesis, ETH Zürich, 2015.
[48] P. C. Haljan, P. J. Lee, K.-A. Brickman, M. Acton, L. Deslauriers, and C. Monroe, Phys. Rev. A **72**, 062316 (2005).
[49] D. J. Wineland, C. Monroe, W. M. Itano, D. Leibfried, B. E. King, and D. M. Meekhof, J. Res. Natl. Inst. Stand. Technol. **103**, 259 (1998).
[50] C. Flühmann, V. Negnevitsky, M. Marinelli, and J. P. Home, Phys. Rev. X **8**, 021001 (2018).
[51] S. Popescu, Nat. Phys. **6**, 151 (2010).
[52] A. Asadian, C. Brukner, and P. Rabl, Phys. Rev. Lett. **112**, 190402 (2014).
[53] D. Kienzler, H.-Y. Lo, B. Keitch, L. de Clercq, F. Leupold, F. Lindenfelser, M. Marinelli, V. Negnevitsky, and J. P. Home, Science **347**, 53 (2015).
[54] Z. Hradil, J. Rehacek, J. Fiurasek, and M. Jezek, in *Quantum State Estimation*, Lecture Notes in Physics Vol. 649 (Springer, Berlin, Heidelberg, 2004).
[55] N. Dangniam and C. Ferrie, J. Phys. A **48**, 115305 (2015).
[56] B. L. Schumaker, Phys. Rep. **135**, 317 (1986).
[57] S. L. Braunstein and P. van Loock, Rev. Mod. Phys. **77**, 513 (2005).
[58] P. Campagne-Ibarcq, A. Eickbusch, S. Touzard, E. Zalys-Geller, N. E. Frattini, V. V. Sivak, P. Reinhold, S. Puri, S. Shankar, R. J. Schoelkopf, L. Frunzio, M. Mirrahimi, and M. H. Devoret, arXiv:1907.12487.
[59] J. Cullum, SIAM J. Numer. Anal. **8**, 254 (1971).
[60] R. S. Anderssen and P. Bloomfield, Numer. Math. **22**, 157 (1974).
[61] A. V. Oppenheim, A. S. Willsky, and N. H. S, *Signals and Systems* 2nd ed. (Pearson Education Limited, Harlow, 2014).
[62] O. Landon-Cardinal, L. C. G. Govia, and A. A. Clerk, Phys. Rev. Lett. **120**, 090501 (2018).